Anti-Stokes resonant x-ray Raman scattering for atom specific and excited state selective dynamics

2016 New J. Phys. 18 103011

(http://iopscience.iop.org/1367-2630/18/10/103011)

New Journal of Physics
The open access journal at the forefront of physics

Deutsche Physikalische Gesellschaft DPG
IOP Institute of Physics

Published in partnership with: Deutsche Physikalische Gesellschaft and the Institute of Physics

OPEN ACCESS

RECEIVED
22 April 2016

REVISED
30 August 2016

ACCEPTED FOR PUBLICATION
8 September 2016

PUBLISHED
7 October 2016

PAPER

Anti-Stokes resonant x-ray Raman scattering for atom specific and excited state selective dynamics

Kristjan Kunnus[1,2,11], Ida Josefsson[3], Ivan Rajkovic[4,12], Simon Schreck[1,2,13], Wilson Quevedo[1], Martin Beye[1,14], Sebastian Grübel[4,15], Mirko Scholz[4,16], Dennis Nordlund[5], Wenkai Zhang[6,17], Robert W Hartsock[6], Kelly J Gaffney[6], William F Schlotter[7], Joshua J Turner[7], Brian Kennedy[1], Franz Hennies[8], Simone Techert[4,9,10], Philippe Wernet[1], Michael Odelius[3] and Alexander Föhlisch[1,2]

[1] Institute for Methods and Instrumentation for Synchrotron Radiation Research, Helmholtz-Zentrum Berlin GmbH, Albert-Einstein-Str. 15, D-12489 Berlin, Germany
[2] Institut für Physik und Astronomie, Universität Potsdam, Karl-Liebknecht-Str. 24/25, D-14476 Potsdam, Germany
[3] Department of Physics, Stockholm University, AlbaNova University Centre, SE-10691 Stockholm, Sweden
[4] Max Planck Institute for Biophysical Chemistry, Am Fassberg 11, D-37070 Göttingen, Germany
[5] Stanford Synchrotron Radiation Lightsource, SLAC National Accelerator Laboratory, Menlo Park, CA 94025, USA
[6] PULSE Institute, SLAC National Accelerator Laboratory, Menlo Park, CA 94025, USA
[7] Linac Coherent Light Source, SLAC National Accelerator Laboratory, Menlo Park, CA 94025, USA
[8] MAX-lab, PO Box 118, SE-221 00 Lund, Sweden
[9] Institute for x-ray Physics, Göttingen University, Friedrich Hund Platz 1, D-37077 Göttingen, Germany
[10] Structural Dynamics of (Bio)chemical Systems, DESY, Notkestr. 85, D-22607 Hamburg, Germany
[11] Current address: PULSE Institute, SLAC National Accelerator Laboratory, Menlo Park, CA 94025, USA.
[12] Current address: Stanford Synchrotron Radiation Lightsource, SLAC National Accelerator Laboratory, Menlo Park, CA 94025, USA.
[13] Current address: Stockholm University, Department of Physics, AlbaNova University Center, SE-10691, Sweden.
[14] Current address: FS-FLASH, DESY, Notkestr. 85, D-22607 Hamburg, Germany.
[15] Current address: Swiss Light Source, Paul Scherrer Institut, 5232 Villigen PSI, Switzerland.
[16] Current address: Universität Siegen, Adolf-Reichwein-Str. 2, D-57076 Siegen, Germany.
[17] Current address: Ultrafast Optical Processes Laboratory, Department of Chemistry, University of Pennsylvania, Philadelphia, PA 19104, USA.

E-mail: alexander.foehlisch@helmholtz-berlin.de

Keywords: ultrafast photochemistry, excited state selectivity, anti-Stokes resonant x-ray raman scattering, free electron lasers, resonant inelastic x-ray scattering

Abstract

Ultrafast electronic and structural dynamics of matter govern rate and selectivity of chemical reactions, as well as phase transitions and efficient switching in functional materials. Since x-rays determine electronic and structural properties with elemental, chemical, orbital and magnetic selectivity, short pulse x-ray sources have become central enablers of ultrafast science. Despite of these strengths, ultrafast x-rays have been poor at picking up excited state moieties from the unexcited ones. With time-resolved anti-Stokes resonant x-ray Raman scattering (AS-RXRS) performed at the LCLS, and *ab initio* theory we establish background free excited state selectivity in addition to the elemental, chemical, orbital and magnetic selectivity of x-rays. This unparalleled selectivity extracts low concentration excited state species along the pathway of photo induced ligand exchange of $Fe(CO)_5$ in ethanol. Conceptually a full theoretical treatment of all accessible insights to excited state dynamics with AS-RXRS with transform-limited x-ray pulses is given—which will be covered experimentally by upcoming transform-limited x-ray sources.

With the rapid evolution of sub-picosecond and femtosecond x-ray sources and particularly with the emergence x-ray free-electron lasers, first steps to join the unique electronic structure information of x-ray spectroscopy with the ultrafast time scale of dynamics in matter have been taken [1–8]. Often though, time resolved x-ray spectroscopy at these dilute transient species with x-ray absorption, x-ray fluorescence or electron spectroscopy suffer often from the difficult separation between the overlapping spectral signatures of the dilute excited state species and the ground state. To reach improved chemical selectivity with x-ray lasers nonlinear and

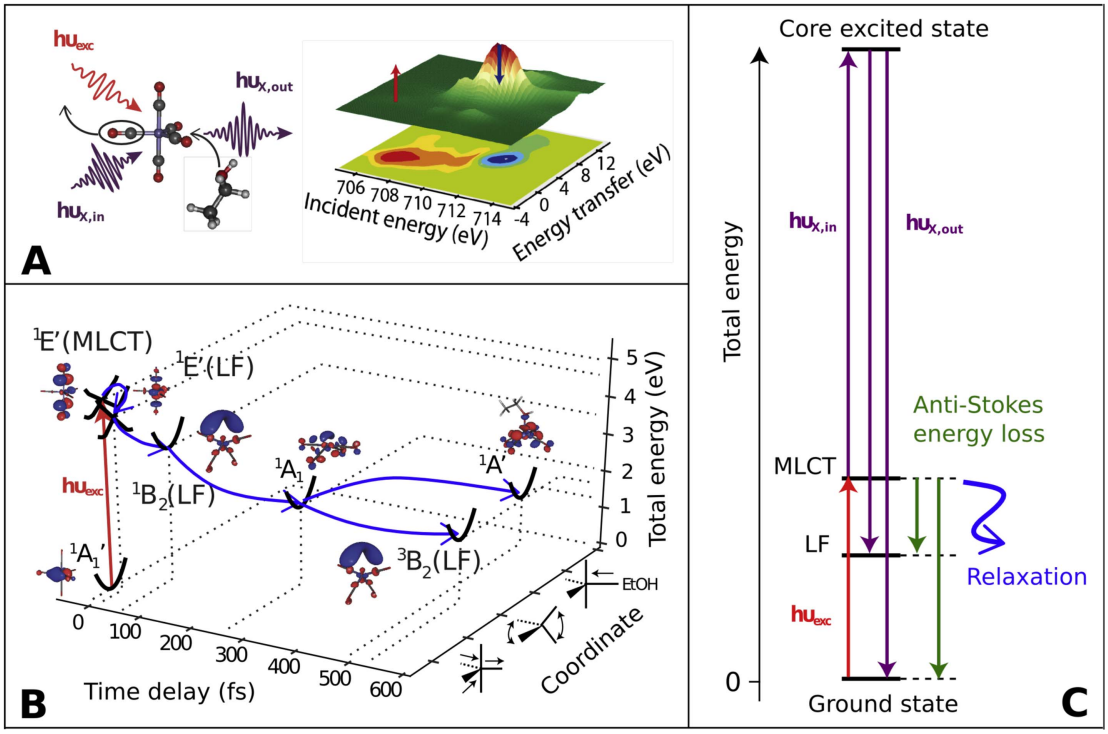

Figure 1. Photo-induced ligand substitution of $Fe(CO)_5$ in ethanol solution into $Fe(CO)_4EtOH$ and its relation to AS-RXRS. (A) Depiction of ligand substitution and AS-RXRS at the Fe L_3 edge. (B) Reaction pathway involving the electronic ground states of $Fe(CO)_5$ $^1A_1'$, $Fe(CO)_4$ $^1A_1$, $Fe(CO)_4$ $^3B_2$, $Fe(CO)_4EtOH$ $^1A'$ and the electronically excited states of $Fe(CO)_5$ $^1E'$ (MLCT), $Fe(CO)_5$ $^1E'$ (LF), and $Fe(CO)_4$ $^1B_2$ (LF), based on [28, 29] that are in this work selectively detected by AS-RXRS. For each state the molecular orbital occupied by the active (highest energy) electron is shown. (C) Mechanism of AS-RXRS in a total energy picture.

multidimensional approaches have been explored both theoretically and experimentally [9–15]. In this work, we show how anti-Stokes resonant x-ray Raman scattering (AS-RXRS) adds unique excited state selectivity to already highly selective resonant inelastic x-ray scattering (RIXS) technique. In recent years, RIXS as a resonantly driven Stokes x-ray Raman process has gradually reached relevant energy scales [16–18] to map out magnetic [19], charge [20], orbital [21] and structural excitations [22, 23] as well as complex potential energy surfaces [24, 25] of functional materials and chemical processes. Additionally, stimulated x-ray Raman scattering was recently used to enhance the RIXS signals [26, 27].

To establish AS-RXRS we use the photochemical pathway of the photoinduced ligand exchange reaction of $Fe(CO)_5$ in ethanol solution (figure 1(A)) and conduct AS-RXRS at the Fe L_3-edge of the electronically excited $Fe(CO)_5$ and $Fe(CO)_4$ species transiently present along the reaction pathway toward the ligand substituted $Fe(CO)_4EtOH$ (figure 1(B)) [28, 29]. This dynamic pathway has been introduced for the gas phase by Trushin *et al* in [30] and modified for ethanol solution by the mechanism of ultrafast ligand addition and spin crossover by previous work of the authors [28, 29]. Cascading dynamics of electronically excited states in $Fe(CO)_5$ is initiated by resonant absorption of a 266 nm (4.66 eV) photon. The initial photo-absorption creates a metal-to-ligand charge-transfer (MLCT) $^1E'$ state which due to Jahn–Teller-like nuclear dynamics converts through possibly multiple internal conversions to a ligand field (LF) $^1E'$ state with a time constant of 21 fs [30]. The conversion therefore includes a relaxation of an electron from delocalized $2\pi^*$ orbital to localized d_σ^* orbital (electron back-transfer). Since d_σ^* is strongly σ-antibonding with respect to the Fe-CO bond, a Jahn–Teller-like motion on the $^1E'(LF)$ surface leads to a transition state (15 fs) which is followed by a dissociation of a single CO ligand and the creation of $Fe(CO)_4$ in an excited $^1B_2(LF)$ state (30 fs) [30]. This electronically excited state evolution we summarize as $^1E'(MLCT) \rightarrow {}^1E'(LF)$ and $^1E'(LF) \rightarrow {}^1B_2(LF)$, with 20 fs and 45 fs time constants, respectively (figure 1(B)). Later, ultrafast ligand addition, spin crossover and geminate recombination finally leads to a branching from the vibrationally hot $Fe(CO)_4$ $^1A_1$ that is in the electronic ground state to the ground state ligand substituted complex $Fe(CO)_4EtOH$ and the picosecond lived high spin $Fe(CO)_4$ $^3B_2$ state [30]. The electronically excited states involved ($^1E'(MLCT)$, $^1E'(LF)$ and $^1B_2(LF)$) can lead in resonant x-ray Raman Scattering to the emission of x-ray photons with an energy higher than the incident x-ray photon energy ($h\upsilon_{X,out} > h\upsilon_{X,in}$), which is the anti-Stokes Raman signature in this x-ray analog to optical time-resolved resonant Raman spectroscopy. As depicted in figure 1(C) this AS-RXRS energy transfer/anti-Stokes shift corresponds to the valence electronic excitation energies.

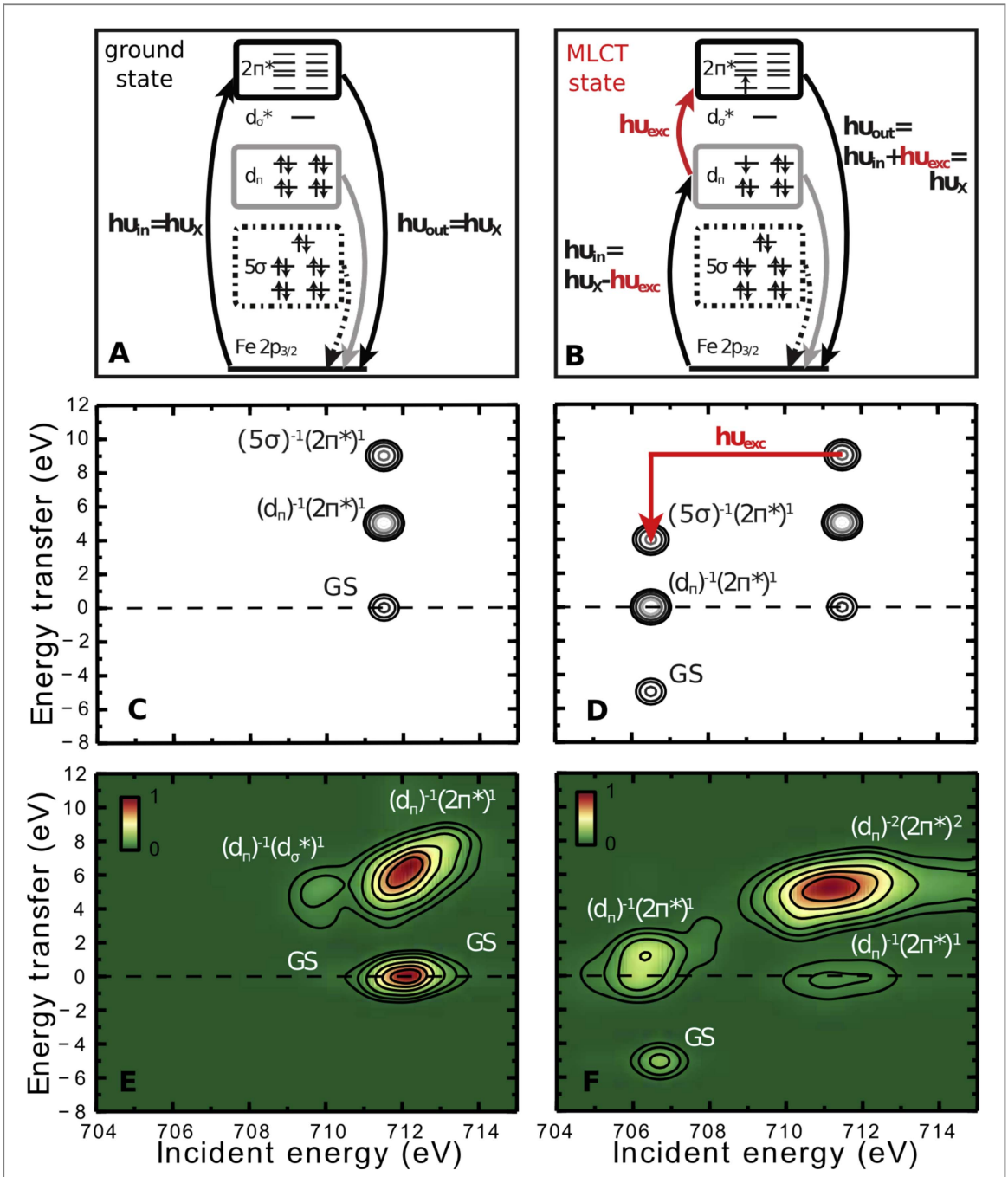

Figure 2. Excited state selectivity of anti-Stokes resonant Raman scattering left column; electronic ground state, right column; additional optically created MLCT excitation. (A) Molecular orbital structure of $Fe(CO)_5$ showing relevant orbitals for Fe L_3-edge RIXS and one-electron transitions through $2\pi^*$ core resonance for the electronic ground state (GS). (B) One-electron transitions involved in the pump-probe anti-Stokes scattering of the optically populated $^1E'[MLCT, (d_\pi)^{-1}(2\pi^*)^1]$ excited state. (C) Schematic $Fe(CO)_5$ ground state RIXS map at the $2\pi^*$ resonance (711.5 eV) based on the MO structure of the complex ($d\sigma^*$ resonance is omitted for clarity). (D) Schematic RIXS map of the $(d_\pi)^{-1}(2\pi^*)^1$ MLCT excited state showing scattering through $2\pi^*$ resonance (711.5 eV) and through d_π hole (706.5 eV) which leads to anti-Stokes scattering (peak at −5 eV energy transfer). (E) Calculated RIXS map of the ground state and (F) the $^1E'[MLCT, (d_\pi)^{-1}(2\pi^*)^1]$ excited state. $(5\sigma)^{-1}(d\sigma^*)^1$ and $(5\sigma)^{-1}(2\pi^*)^1$ final states were not included in the calculations. Labels next to scattering features show the final state.

Results

In figure 2 we show on the left side panels the electronic orbital structure of ground state $Fe(CO)_5$ (figure 2(A)) and how the Stokes resonant x-ray Raman scattering (also commonly denoted as resonant inelastic x-ray scattering, RIXS) leads in the schematic representation of the inelastic x-ray scattering plane (figure 2(C)) to a participator channel with zero energy transfer, and to Stokes energy transfer (loss) due to the creation of final state electron–hole pairs. In figure 2(E) the RIXS map of the $Fe(CO)_5$ ground state calculated with *ab initio* restricted active space self-consistent field (RASSCF) method [31] is shown (see methods for further details). On

the right-hand side panels (B) and (D) of figure 2, we describe how in an one-electron orbital picture the creation of an initial electronic MLCT excitation through optical absorption leads to the opening of a lower energy scattering resonance and the occurrence of fully separated AS-RXRS spectral signatures. Different from the ground state, the optically excited $Fe(CO)_5$ $^1E'$(MLCT) state has a valence vacancy in the d_π orbital. Thus a new energetically lower x-ray scattering resonance is opened up, depicted in figure 2(D). Resonant x-ray Raman Scattering through this excited state resonance occurs at a $h\nu_{exc}$-red-shifted core-level resonance energy and leads for all electron–hole pair final states to the appearance of inelastic scattering features with $h\nu_{exc}$-blue-shifted emission energies in relation to the ground state situation. This is the signature of AS-RXRS. The Resonant x-ray Raman Scattering planes calculated using the RASSCF method in the ground state and in the $^1E'$ (MLCT) excited state in figures 2(E) and (F) confirm the conceptual reasoning based on the simplified one-electron orbitals. Therefore the AS-RXRS spectral features are a result of excitation to the d_π vacancy that is followed by a decay of the excited electrons at the $2\pi^*$ orbital. The most intense AS-RXRS peak in figure 2(F) is at -5 eV energy transfer which corresponds to scattering to the $^1A_1'$ ground state. Dipole selection rules apply to all the involved transitions (pump and probe) and we note that in case of molecules with inversion symmetry, anti-Stokes scattering from optically populated state to the ground state is dipole forbidden. This is not the case for $Fe(CO)_5$ which belongs to the D_{3h} point group symmetry and thus has no inversion center.

In figure 3 we show all AS-RXRS maps of the excited states along the $Fe(CO)_5$ photodissociation pathway. The projections through the scattering planes (white dashed regions) in the AS-RXRS region yield the computed AS-RXRS matching the experimental ones. In particular, we can define spectral regions R1, R2, R3 (black solid regions) that detect background-free the AS-RXRS features of electronically excited states $^1E'$(MLCT) $Fe(CO)_5$, $^1E'$(LF) $Fe(CO)_5$ and $^1B_2$(LF) $Fe(CO)_4$, respectively. In addition (R4) picks up the $^3B_2$(LF) $Fe(CO)_4$ electronic ground state reached after CO detachment. Transient occupation of these states is shown on the right-hand side panels of figure 3. We note that computational treatment of AS-RXRS from different excited molecules have been done before by Tanaka *et al* and Pandey *et al* [32, 33].

In figure 4 direct comparison of experimental and simulated Fe L_3-edge AS-RXRS signatures along the $Fe(CO)_5$ to $Fe(CO)_4EtOH$ ligand substitution pathway is shown. In the panel (A) of figure 4 the resonant x-ray scattering difference map is shown in the center. Along the axis of incident photon energy we observe the opening of the red-shifted x-ray scattering resonance due to the optically created initial $^1E'$(MLCT) state at -4.6 eV excitation energy equal to the pump photon energy (266 nm). Within this spectral region along the emission energy axis the occurrence of blue-shifted anti-Stokes features occurs. The AS-RXRS region R3 shows the transience of the convoluted temporal resolution and the excited state dynamics. The anti-Stokes intensity disappears after 400 fs, with a deconvoluted exponential time constant of ~100 fs, visible from the delay scans in figure 4(A). Region R4 of the $^3B_2$ $Fe(CO)_4$ photoproduct retains significant intensity.

To fully describe the experimental observables (figure 4(A)) through the photochemical pathway of figure 1(B) [28–30], we simulate the observed AS-RXRS features using the RASSCF calculations for all involved excited states from figure 3 and the kinetic rate model of the photochemical pathway (figure 1(B)), taking into account the experimental time resolution of 300 fs and the experimental spectral broadening contributions (figure 4(B), and methods). At these conditions the AS-RXRS feature is dominated by the electronically excited $^1B_2$(LF) state of $Fe(CO)_4$ in region R3 (figure 3(C)). The $^1E'$(MLCT) and $^1E'$(LF) states (with 20 fs and 45 fs lifetimes, respectively) are less pronounced (inset in the simulated RIXS spectrum in figure 4(B)). The $^1B_2$(LF) $Fe(CO)_4$ state correlates with the $^1E'$(LF) $Fe(CO)_5$ state, however it has significantly lower energy due to strong structural relaxation which has taken place (i.e. CO dissociation): based on the RASSCF calculation, the $^1E'$(LF) state is 4.6 eV above the $Fe(CO)_5$ ground state, whereas the relaxed $^1B_2$(LF) state has only ~1 eV higher energy compared to the $Fe(CO)_4$ $^1A_1$ state. Thus this energy relaxation leads to the AS-RXRS feature with a smaller blue shift in comparison to the initial optical excitation energy of $h\nu_{exc} = 4.66$ eV. Simulation of the AS-RXRS feature at 706–707 eV incident photon energy region in figure 4(B) reproduces remarkably well the experimental spectral shape (note that RASSCF calculations at the $2\pi^*$ core resonance at 710–714 eV are less accurate). The lifetime of $^1B_2$(LF) state is ~100 fs and it relaxes via two parallel process to the $^3B_2$(LF) ground state of four-coordinated $Fe(CO)_4$ or to the $^1A_1$ ground state of five-coordinated $Fe(CO)_4L$ (L = EtOH, CO) [21]. This results in disappearance of the anti-Stokes scattering feature (region R3), whereas considerably intensity close to elastic peak at 706–707 eV (region R4) remains due to the $^3B_2$(LF) $Fe(CO)_4$ state (figure 3(D)).

Discussion

We can now demonstrate in figure 5 the full potential of AS-RXRS with transform-limited Gaussian x-ray pulses ($\Delta E\Delta t = 0.44$ h) from upcoming x-ray lasers [34, 35]. Three prototypical scenarios focusing on the initial electron back-transfer between the $Fe(CO)_5$ $^1E'$(MLCT) and 1E′(LF) states and subsequent CO removal during $^1E'$(LF) to $^1B_2$(LF) inter conversion are presented. As defined in figure 3, anti-Stokes features of the $^1E'$(MLCT),

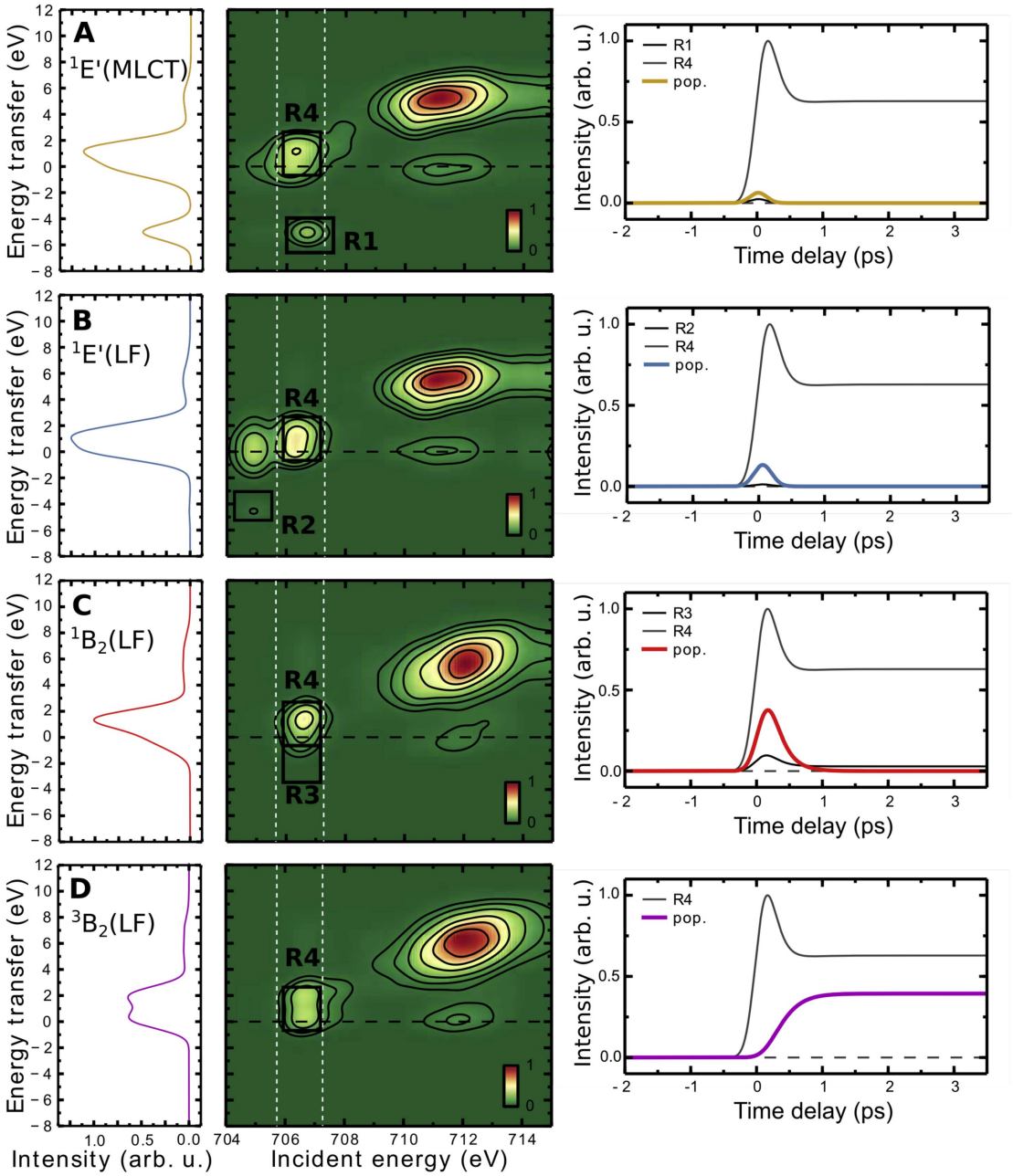

Figure 3. Computed RASSCF resonant inelastic x-ray scattering maps (center column) of the excited states (A) ^{1}E′(MLCT) Fe(CO)$_5$; (B) ^{1}E′(LF) Fe(CO)$_5$; (C) ^{1}B$_2$(LF) Fe(CO)$_4$ and ground state photoproduct (D) ^{3}B$_2$(LF) Fe(CO)$_4$ using the experimental resolution. Left column: resonant inelastic x-ray scattering spectra extracted for 706–707 eV incident photon energy. Right column shows population dynamics of the respective state (colored lines) and the AS-RXRS intensities of regions R1, R2, R3 selective to the respective excited states (R1) ^{1}E′(MLCT) Fe(CO)$_5$; (R2) ^{1}E′(LF) Fe(CO)$_5$; (R3) ^{1}B$_2$(LF) Fe(CO)$_4$ as well as region R4 picking up the ^{3}B$_2$(LF) ground state of Fe(CO)$_4$.

1E′(LF) and ^{1}B$_2$(LF) states are picked up within R1, R2 and R3, located at −5 eV, −4.6 eV and −1 eV energy transfer, respectively. AS-RXRS preserves the bandwidth ΔE of the scattered radiation at linear dispersion with an upper limit given by the natural core-hole lifetime broadening Γ (0.3 eV at the Fe L_3-edge) reflecting the Fe L_3-edge 2.2 fs natural core-hole lifetime. We give the overall temporal resolution in the simulation as the convolution of probe and pump pulses at delay t (assumed equal in duration). With different pulse length Δt, both the temporal resolution and the chemical selectivity can be varied and finest details of the dynamics and potential energy surfaces of excited states can be extracted background free. Column A of figure 5 shows highest temporal selectivity with a pulse duration of $\Delta t = 1$ fs that separates the ^{1}E′(MLCT) and ^{1}E′(LF) states in time, but with $\Delta E = 2.0$ eV incident bandwidth at the cost of no spectral selectivity. However, the features from the ^{1}E′(MLCT) and ^{1}E′(LF) states can still be well distinguished since increasing the bandwidth beyond the core-hole lifetime broadening does not result in further broadening of the spectra. Column B of figure 5 shows optimized chemical selectivity and temporal resolution through a transform limited pulse with $\Delta E = 0.2$ eV and a pulse

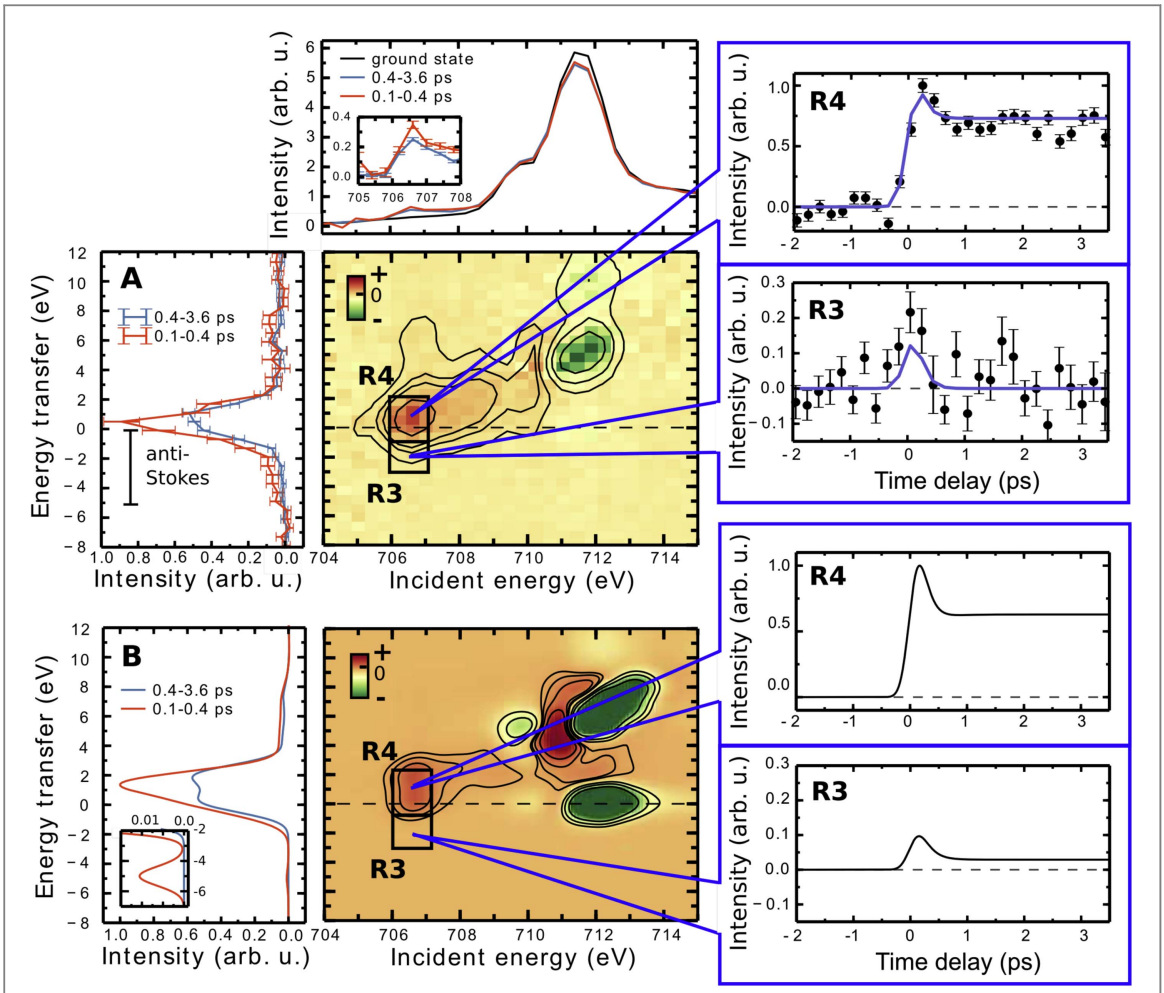

Figure 4. Experimental observation and simulations of AS-RXRS at the Fe L_3-edge the $Fe(CO)_5$ photochemistry. (A) Experiment. Center: pumped–unpumped difference map containing resonant inelastic x-ray scattering and AS-RXRS; top: projection into x-ray absorption spectra: ground state (black line), at time delay 0.1–0.4 ps (red line) and 0.4–3.6 ps (blue line); left: occurrence of AS-RXRS features between −5 and −1 eV energy transfer at 706–707 eV incident energy, that is present at 0.1–0.4 ps time delay; right: temporal evolution of the intensity in AS-RXRS regions showing excited state dynamics. (B) Simulation with RAS-SCF and the kinetic rate model. Center: pumped–unpumped difference; left: difference spectra at 706–707 eV incident energy at 0.1–0.4 ps and 0.4–3.6 ps, inset shows magnification of an AS-RXRS feature corresponding to E′(MLCT) $Fe(CO)_5$ state; right: delay scans from the respective regions.

duration of $\Delta t = 10$ fs. This yields distinction both energetically and temporally and separates AS-RXRS features of the ^{1}E′(MLCT), ^{1}E′(LF) and $^1B_2$(LF) states. Column C of figure 5 shows how sub-natural linewidth resolution maps out the potential energy surfaces [22, 25, 36] of the ^{1}E′(MLCT), ^{1}E′(LF) excited states individually for transform limited pulses with $\Delta E = 0.02$ eV and pulse duration of $\Delta t = 100$ fs. Although no direct temporal separation occurs, the chemical shift between the x-ray scattering resonances of the different ^{1}E′(MLCT), ^{1}E′(LF) excited states separates them, thus allowing to map the potential energy surface of the excited states undergoing rapid photochemical dynamics.

Methods

Computational details

Theoretical x-ray spectra were derived from RASSCF calculations [37] using the MOLCAS-7 software [38]. For further details see [28, 29]. The geometries were optimized with the CASPT2 method [39] and the TZVP basis set [40] for all atoms. The active space contained 12 electrons in 12 orbitals. Some of the geometries were optimized with density functional theory using the PBE functional [41] and the TZVP basis set.

Following experimental factors contribute to the spectral linewidth in the experiment and are taken into account in the simulation of the experiment: the 0.3 eV core-hole lifetime broadening, 0.5 eV incident x-ray bandwidth, 1 eV spectrometer resolution and the 0.5 eV due to inhomogeneous broadening from solvent environment and vibrational effects (all values FWHM). RIXS spectra were simulated using the Kramers–

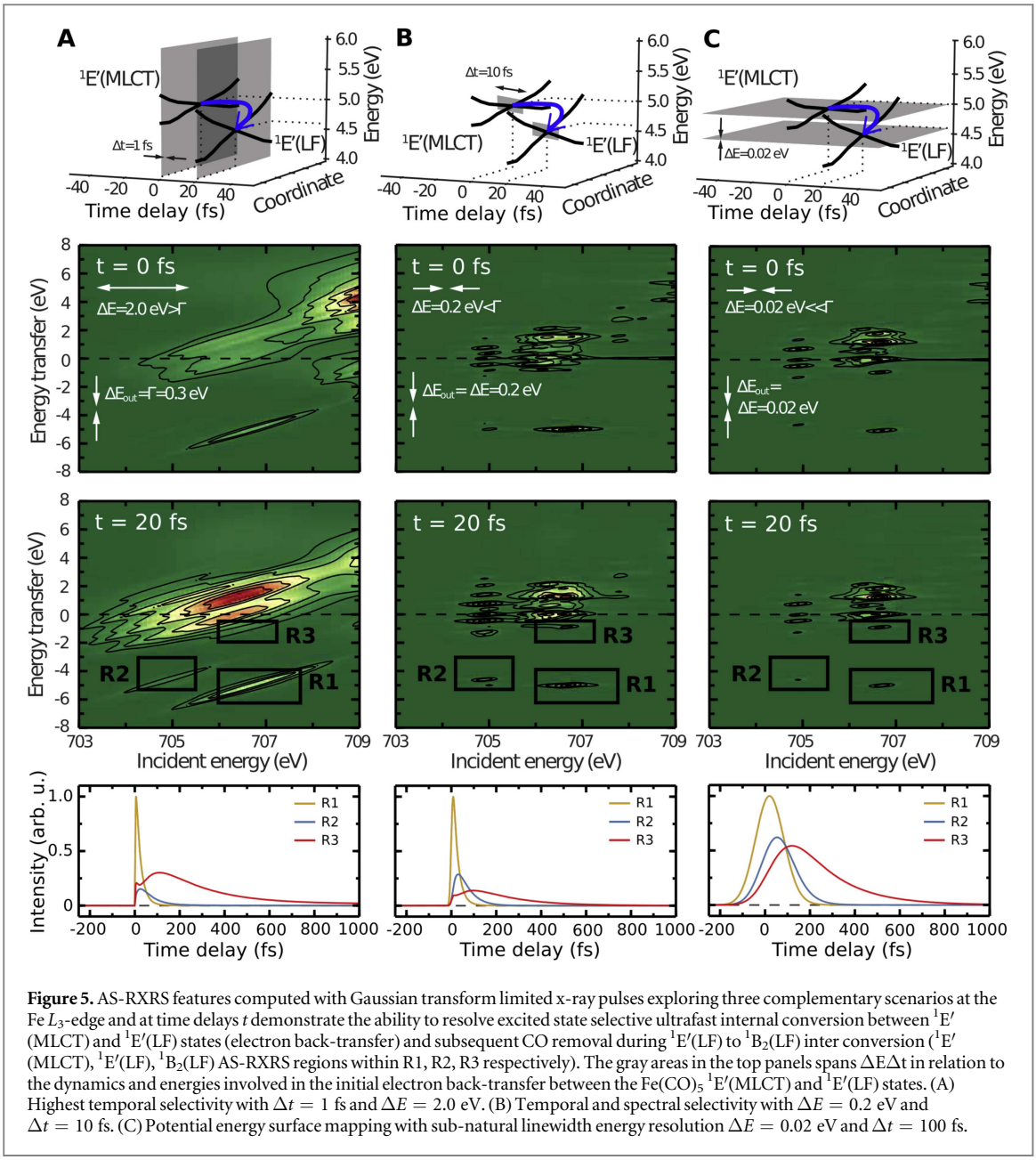

Figure 5. AS-RXRS features computed with Gaussian transform limited x-ray pulses exploring three complementary scenarios at the Fe L_3-edge and at time delays t demonstrate the ability to resolve excited state selective ultrafast internal conversion between ^{1}E′ (MLCT) and ^{1}E′(LF) states (electron back-transfer) and subsequent CO removal during ^{1}E′(LF) to $^1B_2$(LF) inter conversion (^{1}E′ (MLCT), ^{1}E′(LF), $^1B_2$(LF) AS-RXRS regions within R1, R2, R3 respectively). The gray areas in the top panels spans ΔEΔt in relation to the dynamics and energies involved in the initial electron back-transfer between the Fe(CO)$_5$ ^{1}E′(MLCT) and ^{1}E′(LF) states. (A) Highest temporal selectivity with $\Delta t = 1$ fs and $\Delta E = 2.0$ eV. (B) Temporal and spectral selectivity with $\Delta E = 0.2$ eV and $\Delta t = 10$ fs. (C) Potential energy surface mapping with sub-natural linewidth energy resolution $\Delta E = 0.02$ eV and $\Delta t = 100$ fs.

Heisenberg formula. Spectra were calculated for an ensemble of randomly oriented molecules excited by linearly polarized light and detected in the plane of polarization. Interference effects were excluded.

Experimental details

Experiment was performed at the linac coherent light source (LCLS) soft x-ray materials science (SXR) instrument [42, 43] with the liquid jet endsation [44]. The 1 mol l^{-1} Fe(CO)$_5$ ethanol solution was photo-excited at 266 nm (4.66 eV). The pump-laser pulse duration amounted to 100 fs (FWHM) and the pulse energy was estimated to ~5 μJ. With a pump-laser spot size of 100 × 400 μm^2, this corresponded to a peak fluence of ~1.25 × 10^{11} W cm^{-2}. We found no evidence for multi-photon processes at this fluence of the pump laser.

Fe L_3-RIXS intensities were measured by scanning the incident photon energy from 703 to 715 eV. The resolution in the RIXS measurements along the incident-photon energy axis is defined by the excitation bandwidth. This amounted here to 0.5 eV (FWHM) and was determined by the slit size of 150 μm of the SXR monochromator. Incident flux was measured on a shot-by-shot basis using intensity monitor installed after the monochromator [45].

Competing financial interests

The authors declare no competing financial interests.

Acknowledgments

Use of the Linac Coherent Light Source (LCLS), SLAC National Accelerator Laboratory, is supported by the US Department of Energy, Office of Science, Office of Basic Energy Sciences under Contract No. DE-AC02-76SF00515. The SXR Instrument is funded by a consortium whose membership includes the LCLS, Stanford University through the Stanford Institute for Materials Energy Sciences (SIMES), Lawrence Berkeley National Laboratory (LBNL), University of Hamburg through the BMBF priority program FSP 301, and the Center for Free Electron Laser Science (CFEL). Part of this research was conducted within the Helmholtz Virtual Institute VI 419 'Dynamic Pathways in Multidimensional Landscapes'. MO acknowledges support from the Swedish Research Council, Carl Tryggers Foundation, and Magnus Bergvall Foundation. AF acknowledges funding from the ERC-ADG-2014—Advanced Investigator Grant—no. 669531 EDAX under the Horizon 2020 EU Framework Programme for Research and Innovation. The computations were performed on resources provided by the Swedish National Infrastructure for Computing (SNIC) at the Swedish National Supercomputer Center (NSC) and the High Performance Computer Center North (HPC2N). MB had financial support by the Volkswagen Stiftung. IR, WQ, SG, MS and ST are grateful to SFB755-DFG and SFB1073-DFG for financial support. WZ, RWH, and KJG acknowledge support through the AMOS program within the Chemical Sciences, Geosciences, and Biosciences Division of the Office of Basic Energy Sciences, Office of Science, US Department of Energy.

Author contributions

The manuscript was written by KK and AF with input from all co-authors. IJ and MO carried out the RASSCF calculations. KK, IR, SS, WQ, MB, SG, MS, DN, WZ, RWH, KJG, WFS, JJT, BK, FH, ST, PW and AF carried out the experiment.

Additional information

Correspondence and requests for materials should be addressed to AF.

References

[1] Canton S E *et al* 2013 Toward highlighting the ultrafast electron transfer dynamics at the optically dark sites of photocatalysts *J. Phys. Chem. Lett.* **4** 1972–6
[2] Siefermann K R *et al* 2014 Atomic-scale perspective of ultrafast charge transfer at a dye–semiconductor interface *J. Phys. Chem. Lett.* **5** 2753–9
[3] Chergui M and Zewail A H 2009 Electron and x-ray methods of ultrafast structural dynamics: advances and applications *Chem. Phys. Chem.* **10** 28–43
[4] Zhang W *et al* 2014 Tracking excited-state charge and spin dynamics in iron coordination complexes *Nature* **509** 345–8
[5] Bressler C *et al* 2009 Femtosecond XANES study of the light-induced spin crossover dynamics in an iron(II) complex *Science* **323** 489–92
[6] Chergui M 2014 Emerging photon technologies for chemical dynamics *Faraday Discuss.* **171** 11–40
[7] Huse N *et al* 2011 Femtosecond soft x-ray spectroscopy of solvated transition-metal complexes: deciphering the interplay of electronic and structural dynamics *J. Phys. Chem. Lett.* **2** 880–4
[8] Wen H, Huse N, Schoenlein R W and Lindenberg A M 2009 Ultrafast conversions between hydrogen bonded structures in liquid water observed by femtosecond x-ray spectroscopy *J. Chem. Phys.* **131** 234505
[9] Mukamel S, Healion D, Zhang Y and Biggs J D 2013 Multidimensional attosecond resonant x-ray spectroscopy of molecules; lessons from the optical regime *Annu. Rev. Phys. Chem.* **64** 101–27
[10] Adams B 2011 The next phase for x-rays *Nat. Phys.* **7** 675–6
[11] Marcus G, Penn G and Zholents A A 2014 Free-electron laser design for four-wave mixing experiments with soft-x-ray pulses *Phys. Rev. Lett.* **113** 024801
[12] Patterson B D 2010 Resource letter on stimulated inelastic x-ray scattering at an XFEL *SLAC Technical Note* SLAC-TN-10-026
[13] Hara T, Inubushi Y and Katayama T 2013 Two-colour hard x-ray free-electron laser with wide tunability *Nat. Commun.* **4** 2919
[14] Bencivenga F *et al* 2015 Four wave mixing experiments with extreme ultraviolet transient gratings *Nature* **520** 205
[15] Bencivenga F, Capotondi F, Kiskinova M and Masciovecchio C 2015 Four wave mixing experiments with extreme ultraviolet transient gratings *Adv. Phys.* **63** 327
[16] Ghiringhelli G *et al* 2006 SAXES, a high resolution spectrometer for resonant x-ray emission in the 400–1600 eV energy range *Rev. Sci. Instrum.* **77** 113108
[17] Strocov V N *et al* 2010 High-resolution soft x-ray beamline ADRESS at the Swiss Light Source for resonant inelastic x-ray scattering and angle-resolved photoelectron spectroscopies *J. Synchrotron Radiat.* **17** 631–43
[18] Schmitt T *et al* 2013 High-resolution resonant inelastic x-ray scattering with soft x-rays at the {ADRESS} beamline of the Swiss Light Source: instrumental developments and scientific highlights *J. Electron Spectrosc. Relat. Phenom.* **188** 38–46
[19] Ghiringhelli G and Braicovich L 2013 Magnetic excitations of layered cuprates studied by RIXS at Cu L_3 edge *J. Electron Spectrosc. Relat. Phenom.* **188** 26–31
[20] Ament L J P, van Veenendaal M, Devereaux T P, Hill J P and van den Brink J 2011 Resonant inelastic x-ray scattering studies of elementary excitations *Rev. Mod. Phys.* **83** 705–67

[21] Schlappa J et al 2012 Spin–orbital separation in the quasi-one-dimensional mott insulator Sr_2CuO_3 Nature 485 82–5
[22] Hennies F et al 2010 Resonant inelastic scattering spectra of free molecules with vibrational resolution Phys. Rev. Lett. 104 193002
[23] Pietzsch A et al 2011 Spatial quantum beats in vibrational resonant inelastic soft x-ray scattering at dissociating states in oxygen Phys. Rev. Lett. 106 153004
[24] Sun Y-P et al 2011 Internal symmetry and selection rules in resonant inelastic soft x-ray scattering J. Phys. B: At. Mol. Opt. Phys. 44 161002
[25] Schreck S et al 2016 Ground state potential energy surfaces around selected atoms from resonant inelastic x-ray scattering Nat. Sci. Rep. 7 20054
[26] Beye M et al 2013 Stimulated x-ray emission for materials science Nature 501 191–4
[27] Schreck S, Beye M and Föhlisch A 2015 Implications of stimulated resonant x-ray scattering for spectroscopy, imaging, and diffraction in the regime from soft to hard x-rays J. Mod. Opt. 62 S41–51
[28] Wernet P et al 2015 Orbital-specific mapping of the ligand exchange dynamics of $Fe(CO)_5$ in solution Nature 520 78–81
[29] Kunnus K et al 2016 Identification of the dominant photochemical pathways and mechanistic insights to the ultrafast ligand exchange of $Fe(CO)_5$ to $Fe(CO)_4EtOH$ Struct. Dyn. 3 043204
[30] Trushin S A, Fuß W, Kompa K L and Schmid W E 2000 Femtosecond dynamics of $Fe(CO)_5$ photodissociation at 267 nm studied by transient ionization J. Phys. Chem. A 104 1997–2006
[31] Josefsson I et al 2012 Ab initio calculations of x-ray spectra: atomic multiplet and molecular orbital effects in a multiconfigurational scf approach to the L-edge spectra of transition metal complexes J. Phys. Chem. Lett. 3 3565–70
[32] Tanaka S, Volkov S and Mukamel S 2003 Time-resolved x-ray Raman spectroscopy of photoexcited polydiacetylene oligomer: a simulation study J. Chem. Phys. 118 3065
[33] Pandey R K and Mukamel S 2006 Simulation of x-ray absorption near-edge spectra and x-ray fluorescence spectra of optically excited molecules J. Chem. Phys. 124 094106
[34] Allaria E et al 2012 Highly coherent and stable pulses from the FERMI seeded free-electron laser in the extreme ultraviolet Nat. Photon. 6 699–704
[35] Allaria E et al 2013 Two-stage seeded soft-x-ray free-electron laser Nat. Photon. 7 913–8
[36] Sun Y-P et al 2011 Intramolecular soft modes and intermolecular interactions in liquid acetone Phys. Rev. B 84 132202
[37] Malmqvist P Å, Rendell A and Roos B O 1990 The restricted active space self-consistent-field method, implemented with a split graph unitary-group approach J. Phys. Chem. 94 5477–82
[38] Aquilante F et al 2010 Software news and update MOLCAS 7: the next generation J. Comput. Chem. 31 224–47
[39] Finley J, Malmqvist P A, Roos B O and Serrano-Andres L 1998 The multi-state CASPT2 method Chem. Phys. Lett. 288 299–306
[40] Schafer A, Huber C and Ahlrichs R 1994 Fully optimized contracted gaussian-basis sets of triple zeta valence quality for atoms Li to Kr J. Chem. Phys. 100 5829–35
[41] Perdew J P, Burke K and Ernzerhof M 1996 Generalized gradient approximation made simple Phys. Rev. Lett. 77 3865–8
[42] Schlotter W F et al 2012 The soft x-ray instrument for materials studies at the linac coherent light source x-ray free-electron laser Rev. Sci. Instrum. 83 43107
[43] Dakovski G L et al 2015 The soft x-ray research instrument at the linac coherent light source J. Synchrotron Radiat. 22 498–502
[44] Kunnus K et al 2012 A setup for resonant inelastic soft x-ray scattering on liquids at free electron laser light sources Rev. Sci. Instrum. 83 123109
[45] Tiedtke K et al 2014 Absolute pulse energy measurements of soft x-rays at the linac coherent light source Opt. Express 22 21214